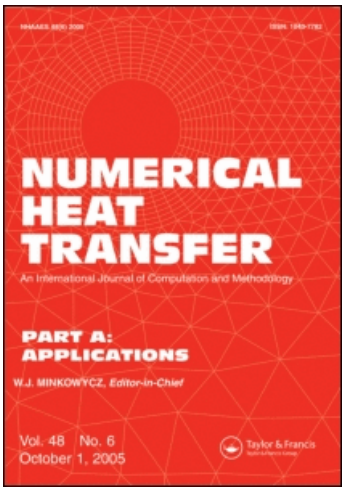

Numerical Heat Transfer, Part A: Applications
Publication details, including instructions for authors and subscription information:
http://www.informaworld.com/smpp/title~content=t713657973

A Node-based Smoothed Point Interpolation Method (NS-PIM) for Three-dimensional Thermoelastic Problems

S. C. Wu [ab]; G. R. Liu [bc]; H. O. Zhang [a]; G. Y. Zhang [c]
[a] State Key Laboratory of Digital Manufacturing and Equipment Technology, Huazhong, University of Science and Technology, Wuhan, People's Repulic of China [b] Centre for Advanced Computations in Engineering Science (ACES), Department of Mechanical Engineering, National University of Singapore, Singapore [c] Singapore-MIT Alliance (SMA), Singapore

Online Publication Date: 01 January 2008

To cite this Article Wu, S. C., Liu, G. R., Zhang, H. O. and Zhang, G. Y.(2008)'A Node-based Smoothed Point Interpolation Method (NS-PIM) for Three-dimensional Thermoelastic Problems',Numerical Heat Transfer, Part A: Applications,54:12,1121 — 1147
To link to this Article: DOI: 10.1080/10407780802483516
URL: http://dx.doi.org/10.1080/10407780802483516

Numerical Heat Transfer, Part A, 54: 1121–1147, 2008

ISSN: 1040-7782 print/1521-0634 online
DOI: 10.1080/10407780802483516

A NODE-BASED SMOOTHED POINT INTERPOLATION METHOD (NS-PIM) FOR THREE-DIMENSIONAL THERMOELASTIC PROBLEMS

S. C. Wu[1,2], G. R. Liu[2,3], H. O. Zhang[1], and G. Y. Zhang[3]

[1]*State Key Laboratory of Digital Manufacturing and Equipment Technology, Huazhong, University of Science and Technology, Wuhan, People's Repulic of China*

[2]*Centre for Advanced Computations in Engineering Science (ACES), Department of Mechanical Engineering, National University of Singapore, Singapore*

[3]*Singapore-MIT Alliance (SMA), Singapore*

A node-based smoothed point interpolation method (NS-PIM) is formulated to analyze 3-D steady-state thermoelastic problems subjected to complicated thermal and mechanical loads. Gradient smoothing technique with node-based smoothing domains is utilized to modify the gradient fields and to perform the numerical integration required in the weak form formulation. Numerical results show that NS-PIM can achieve more accurate solutions even when the 4-node tetrahedral mesh is used compared to the finite-element method (FEM) using the same mesh, especially for strains and hence stresses. Most importantly, it can produce an upper bound solution of the exact solution in energy norm for both temperature and stress fields when a reasonably fine mesh is used. Together with FEM, we now for the first time have a simple means to obtain both upper and lower bounds of the exact solution to complex thermoelastic problems.

1. INTRODUCTION

Recently, meshfree methods [1] have been developed as the powerful alternative techniques to the finite-element method (FEM) [2–4], and remarkable progress has been made in providing more accurate and even upper bound solutions to the exact ones in energy norms [5]. Widely used meshfree methods include the smoothed particle hydrodynamic method (SPH) [6, 7], the element-free Galerkin method (EFG) [8], the reproducing kernel particle method (RKPM) [9], the meshless local Petrov-Galerkin method (MLPG) [10], and the point interpolation method (PIM) [1], etc.

Received 29 July 2008; accepted 3 September 2008.

The support of the National Natural Science Foundation of China under project No. 50474053, 50475134, and 50675081 along with the 863 project (No. 2007AA04Z142) are gratefully acknowledged. The authors also give sincere thanks to the support of the Centre for ACES, the Singapore-MIT Alliance (SMA), and the National University of Singapore.

Address correspondence to S. C. Wu, State Key Laboratory of Digital Manufacturing and Equipment and Technology, School of Mechanical Science and Engineering, Huazhong University of Science and Technology, Wuhan 430074, PR China. E-mail: wushengchuan@gmail.com

NOMENCLATURE

$\mathbf{a}$	The vector of unkown coefficients	$\boldsymbol{\sigma}, \boldsymbol{\varepsilon}, \boldsymbol{\varepsilon}_0$	cauchy stress and strain, initial strain
$\mathbf{d}$	nodal displacement vector	$\bar{\boldsymbol{\sigma}}, \bar{\boldsymbol{\varepsilon}}$	smoothed stress and strain
h	convection coefficient, $W/(m^2 \cdot {}^\circ C)$	δ, ∇	variational and gradient symbol
k_i	thermal conductivity, $W/(m \cdot {}^\circ C)$	α	thermal expansion, $1/{}^\circ C$
Q_v	internal heat source, W/m^3	Ω	integration or problem domain
q_Γ	prescribed heat flux, W/m^2	Γ	global or local boundary
t_Γ	given traction, N/m^2		Subscripts and superscripts
T_Γ	specified temperature, $^\circ C$	i, I, J	tensor or node indices
T_a	known ambient temperature, $^\circ C$	k	smoothing domain for node k
u_Γ	given displacement, m	d	thermal strain energy, J
$\boldsymbol{\Phi}$	vector of PIM shape functions	T, T	transpose symbol and energy indicator

The node-based smoothed PIM (NS-PIM or LC-PIM termed originally [11]) is found very stable (spatially), works well with triangular types of mesh, is free from volumetric locking, and capable of producing upper bound solutions [5] in a very convenient manner using the same mesh as that used in standard FEM. The NS-PIM was developed using shape functions constructed using simple point interpolation through a set of arbitrarily scattered nodes within a local support domain [12]. Both polynomial PIM [1] and radial PIM (RPIM) [13] of Delta function property can be used in the NS-PIM, which allows the straightforward imposition of essential boundary conditions. NS-PIM or (NS-RPIM [14]) was originally formulated for 2-D [11] and 3-D [15] elasticity problems with a more accurate stress solution and is more tolerant to mesh distortion, using the generalized gradient smoothing technique [16] that was extended from the gradient smoothing technique [17] with nodal integration scheme [18]. Therefore, NS-PIM allows incompatible displacement fields [16, 26]. The NS-PIM was then developed for 3-D heat transfer [19] and 2-D thermoelasticity problems [20].

The NS-PIM or NS-RPIM can ensure at least linear consistency and hence the convergence to the exact solution, and possesses a very important property of upper bound solutions for elasticity problems [5, 21]. The theoretical aspects of upper bound can be found in ref. [5]. Such properties for solution bounds in both temperature and equivalent energy norms have also been observed numerically through a number of heat transfers [19] and thermoelastic problems [20]. The NS-PIM works very efficiently with triangular and tetrahedral meshes that can be generated automatically for easily adaptive analysis of complicated geometries [22, 23]. The NS-PIM has also been proven to give a much higher convergence rate of up to 1.5 in energy norm (observed as superconvergence [24]), in contrast to 1.0 which is the highest possible rate for fully compatible linear FEM. The NS-PIM is also known as a semi-equilibrium model for its properties of superconvergence in energy norm, immunity to volumetric locking, and satisfaction to equilibrium equations within all of the smoothing domains [5].

Based on the idea of NS-PIM, a node-based smoothed FEM (NS-FEM) [25] has also been formulated. The NS-FEM can be viewed as a special case of the NS-PIM and n-side polygonal element meshes can be used. It uses compatible displacement fields created based on element, and has quite similar properties as

the NS-PIM. It has been found that both NS-PIM and NS-FEM cannot solve dynamic problems due to their "overly-softness" [5, 15, 19, 20] induced by the excessive node-based smoothing operations, which leads to temporal instability (spurious eigenmodes) for solving time-dependent heat transfer and solid mechanics problems.

To tackle this problem, an edge-based smoothed FEM (ES-FEM) ES-PIM [40], and SFEM have recently been proposed for problems of solid mechanics [27], plate, and shells [28]. The ES-FEM can produce much more accurate solutions in both the primary variable and its gradient using constant strain triangular and tetrahedral element meshes. It is both partially and temporally stable, no spurious eigenmodes, and hence works well for dynamic problems.

With the increasing interests in optimizing physical processes of rapid heating and solidification, analysis of thermal behaviors including temperature gradients as well as resulted thermal stress becomes more and more important [29, 30]. Experimental study on these kinds of systems is usually very expensive, time-consuming, and practically difficult to obtain detailed results. Numerical means such as the FEM is often preferred for this kind of purpose [31]. However, due to its "overly-stiff" property, significant errors can occur especially in high gradient regions. The "overly-stiff" nature of a full-compatible FEM model results in a lower bound solution to the exact one. In contrast, the "soft" nature of the NS-PIM offers a very useful complementary property of upper bound solution. Thus, the simple combination of the upper bound property of NS-PIM and the lower bound property of FEM [4] can bound the numerical solutions from both sides for complicated realistic problems, as long as a reasonablyfine mesh can be created.

In solving 2-D and 3-D problems with complicated geometries, meshing has always been an important issue [1]. It is the opinion of the authors' group that the ultimate solution to these systems is to use triangular and tetrahedral types of meshes, respectively, for 2-D and 3-D problems. Many meshfree methods [1, 12] and element-based methods [25, 27] have been formulated based onthis consideration.

In this work, the NS-PIM is further extended to 3-D thermoelastic problems involving very complex geometries and complicated boundary conditions, including both thermal and mechanical loads. In they present NS-PIM procedure, we use the four-node tetrahedral elements/cells for 3-D solids analysis that can be generated with ease. PIM shape functions are constructed using a polynomial basis and local supporting nodes are based on these tetrahedral cells. Discretized system equations for problems of heat transfer and thermoelasticity are formulated using the generalized smoothed Galerkin weak form [16]. The accuracy, convergence, and the most important upper bound property of numerical solutions using the NS-PIM are studied in detail in comparison with those obtained using the FEM.

2. PIM SHAPE FUNCTIONS

The polynomial PIM is a finite series representation method for creating shape functions, using a small set of nodes within a local support domain. In the scheme, the problem domain is first discretized with arbitrarily scattered nodes inside the problem domain and on the boundary. The background tetrahedral cells are then formed based on these nodes, as shown in Figure 1.

Consider a continuous function $u(\mathbf{x})$ for our 3-D thermoelastic problem, which is defined in the problem domain Ω bounded by Γ,

$$u^h(\mathbf{x}) = \sum_{i=1}^{n} p_i(\mathbf{x}) a_i = \mathbf{p}^{\mathrm{T}}(\mathbf{x})\mathbf{a} \tag{1}$$

where $p_i(\mathbf{x})$ is a given basis function in the Cartesian coordinate space $\mathbf{x}^{\mathrm{T}} = [x, y, z]$, n is the number of polynomial terms, a_i is the coefficient corresponding to the ith basis and is yet to be determined, and the superscript T stands for transpose operator.

The polynomial basis $\mathbf{p}$ $(\mathbf{x})$ in Eq. (1) is usually built utilizing the Pascal's triangles and a complete basis is generally preferred for the requirement of a possible higher order of consistency. For complete order 1, the polynomial basis function can be written as,

$$\mathbf{p}(\mathbf{x}) = \{\, 1 \quad x \quad y \quad z \,\}^{\mathrm{T}} \tag{2}$$

In order to determine the coefficients a_i, a 3-D sub-domain (often called local support domain) for the interested point at $\mathbf{x}$ is constructed based on the background 4-node tetrahedral cells shown in Figure 1, containing a total of n nodes. The coefficients a_i in Eq. (1) can then be determined by enforcing $u(\mathbf{x})$ to pass through all n nodes, which leads to a set of n equations with each for one node.

$$\left.\begin{aligned} u_1 &= a_1 + a_2 x_1 + a_3 y_1 + a_4 z_1 + \cdots \\ u_2 &= a_1 + a_2 x_2 + a_3 y_2 + a_4 z_2 + \cdots \\ &\vdots \\ u_n &= a_1 + a_2 x_n + a_3 y_n + a_4 z_n + \cdots \end{aligned}\right\} \tag{3}$$

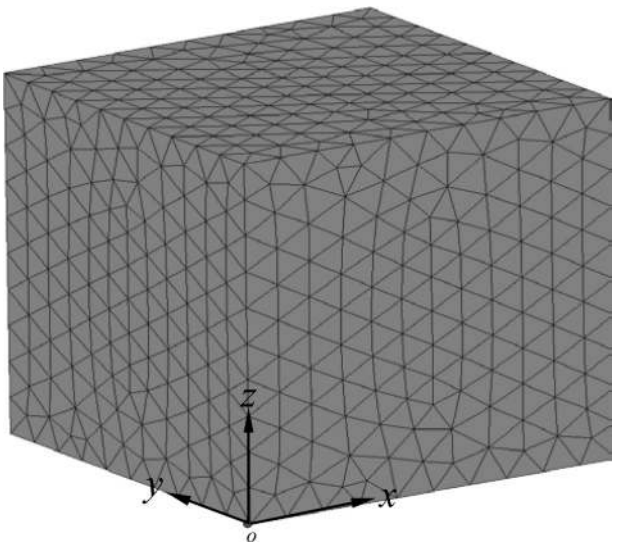

Figure 1. Background 4-node tetrahedral cells for creating PIM shape functions.

Eq. (3) can be written in the matrix form of

$$\mathbf{U}_s = \mathbf{P}\mathbf{a} \tag{4}$$

where $\mathbf{U}_s$ is the nodal displacement vector in the support domain, $\mathbf{a}$ is the vector of unknown coefficients, and $\mathbf{P}$ is the coefficient matrix that can be given,

$$\mathbf{P} = \begin{bmatrix} 1 & x_1 & y_1 & z_1 & \cdots \\ 1 & x_2 & y_2 & z_2 & \cdots \\ 1 & x_3 & y_3 & z_3 & \cdots \\ \vdots & \vdots & \vdots & \vdots & \ddots \\ 1 & x_n & y_n & z_n & \cdots \end{bmatrix}_{n\times n} \tag{5}$$

Note that $\mathbf{P}$ is a square matrix because the number of nodes used in the local support domain is the same as the number of basis functions. If $\mathbf{P}^{-1}$ exists [1, 12], a unique solution for $\mathbf{a}$ can then be obtained as

$$\mathbf{a} = \mathbf{P}^{-1}\mathbf{U}_s \tag{6}$$

Different from the moving least-square approximation [32], coefficients $\mathbf{a}$ here are constants even if the point of interest at $\mathbf{x}$ changes in a local cell of interest where a same set of n nodes are used in the interpolation. Substituting Eq. (6) into Eq. (1) yields

$$u^h(\mathbf{x}) = \mathbf{p}^{\mathrm{T}}(\mathbf{x})\mathbf{P}^{-1}\mathbf{U}_s = \sum_{i=1}^{n} \varphi_i(\mathbf{x})u_i = \Phi^{\mathrm{T}}(\mathbf{x})\mathbf{U}_s \tag{7}$$

where $\Phi(\mathbf{x})$ is a matrix of the PIM shape functions that can be expressed as

$$\Phi^{\mathrm{T}}(\mathbf{x}) = \mathbf{p}^{\mathrm{T}}(\mathbf{x})\mathbf{P}^{-1} = \{\ \varphi_1(\mathbf{x})\varphi_2(\mathbf{x})\cdots\varphi_n(\mathbf{x})\ \} \tag{8}$$

The derivatives of the PIM shape function can be obtained very easily due to its polynomial property, but they are *not* required in the present NS-PIM because it is in fact a W^2 formulation [26]. In addition, shape functions created using the PIM procedure possess the Kronecker Delta function property, which permits simple imposition of essential boundary conditions just as what we do in the FEM.

Note that in this work we only use the linear interpolation. Higher order interpolation and even the radial point interpolation are possible [14, 26]. In such a case, the assumed field function is no longer continuous, belongs to a G space, and hence a more general W^2 formulation based on the G space theory needs to be used to ensure the stability, uniqueness, and the convergence [26].

3. DISCRETIZED SYSTEM EQUATIONS

The 4-node tetrahedral mesh, such as the one shown in Figure 1, is often preferred in engineering analysis and design for 3-D problems with complicated geometry, because this kind of mesh can be generated much more easily in automatic

manners, resulting in significant savings in manpower and hence the cost in the analysis and design process. Additionally, adaptive analysis can be more easily implemented for solutions of desired accuracy [22, 23]. We therefore only use 4-node tetrahedral mesh as background cells for node selection and the PIM shape functions construction. When only four nodes are used in the local interpolation it leads to a set of linear shape functions that are the same as those of the linear FEM. Higher order NS-PIM using 4-node tetrahedral background mesh can be found in ref. [26].

3.1. Governing Equations

Consider a linear static thermoelasticity problem [33, 34] defined in an anisotropic solid Ω bounded by Γ. The governing equations (in the absence of body force) can be given in Ω as,

$$k_x \frac{\partial^2 T}{\partial x^2} + k_y \frac{\partial^2 T}{\partial y^2} + k_z \frac{\partial^2 T}{\partial z^2} + Q_v = 0 \tag{9}$$

$$\nabla \boldsymbol{\sigma} = 0 \tag{10}$$

where T is the unknown field variable of temperature, k_i $(i = x,\ y,\ z)$ is the conductivity of heat in the ith direction, Q_v is an inner heat source, and σ denotes the unknown stress field in the solids.

Three types of possible thermal boundary conditions are given by

$$T = T_\Gamma \quad \text{on } \Gamma_T \quad \text{Specified temperature} \tag{11}$$

$$q_n = q_\Gamma \quad \text{on } \Gamma_q \quad \text{Specified heat flux} \tag{12}$$

$$q_n = h(T - T_a) \quad \text{on } \Gamma_c \quad \text{Convection} \tag{13}$$

where T_Γ is the prescribed temperature, q_Γ is the specified heat flux, h is the convection coefficient, and T_a is the known temperature of the ambient medium.

The solid can also be subjected to mechanical conditions in the form of specified displacements and tractions,

$$\mathbf{u} = u_\Gamma \quad \text{on } \Gamma_u \quad \text{Specified displacement} \tag{14}$$

$$\boldsymbol{\sigma} \cdot \mathbf{n} = t_\Gamma \quad \text{on } \Gamma_t \quad \text{Specified traction} \tag{15}$$

where u_Γ is the prescribed displacement on Γ_u, t_Γ is the given traction on Γ_t, and $\mathbf{n}$ is the vector of unit outward normal on Γ.

3.2. Smoothed Galerkin Weak Form

In the general formulation of NS-PIM, a generalized smoothed bilinear form is used to establish the discretized system equations [16] and weakened weak (W^2) formulation that allows assumed functions residing in a G space (including H space) is used [26]. In this work, to obtain the smoothed Galerkin weak form for heat transfer analysis, the (energy) functional associated with heat equilibrium Eq. (9) and its corresponding boundary conditions of Eqs. (11)–(13) can be first expressed as

$$I(T) = \int_\Omega \frac{1}{2}\left[k_1\left(\frac{\partial T}{\partial x}\right)^2 + k_2\left(\frac{\partial T}{\partial y}\right)^2 + k_3\left(\frac{\partial T}{\partial z}\right)^2 - 2Q_v T\right] d\Omega - \int_{\Gamma_q} q_\Gamma T d\Gamma + \frac{1}{2}\int_{\Gamma_c} h(T - T_a)^2 d\Gamma \tag{16}$$

Here, we require the assumed function for T has squarely integrable first derivatives and hence is in a Hilbert (H) space. The variational form of the thermal system can now be presented as

$$\delta I(T) = \int_\Omega \left[\delta(\nabla T)^{\mathrm{T}} \mathbf{k} \nabla T\right] d\Omega - \int_\Omega \delta T Q_v d\Omega + \int_{\Gamma_q} \delta T q_\Gamma d\Gamma + \int_{\Gamma_c} hT\delta T d\Gamma - \int_{\Gamma_c} hT_a \delta T d\Gamma = 0 \tag{17}$$

where $\mathbf{k}$ and ∇T are defined as

$$\mathbf{k} = \begin{Bmatrix} k_x & 0 & 0 \\ 0 & k_y & 0 \\ 0 & 0 & k_z \end{Bmatrix} \quad \text{and} \quad \nabla T = \begin{Bmatrix} \dfrac{\partial T}{\partial x} & \dfrac{\partial T}{\partial y} & \dfrac{\partial T}{\partial z} \end{Bmatrix}^{\mathrm{T}} \tag{18}$$

The temperature gradient ∇T presented in Eq. (17) is now replaced by the smoothed temperature gradient $\nabla \overline{T}$. The smoothed Galerkin weak form for heat transfer problems can then be obtained as follows.

$$\int_\Omega \delta(\nabla \overline{T})^{\mathrm{T}} \mathbf{k} \nabla \overline{T} d\Omega - \int_\Omega \delta T^{\mathrm{T}} Q_v d\Omega + \int_{\Gamma_q} \delta T^{\mathrm{T}} q_\Gamma d\Gamma + \int_{\Gamma_c} \delta T^{\mathrm{T}} hT d\Gamma - \int_{\Gamma_c} \delta T^{\mathrm{T}} hT_a d\Gamma = 0 \tag{19}$$

Substituting Eq. (7) into Eq. (19), a set of discretized system equations can be built in the following matrix form.

$$[\overline{\mathbf{K}} + \mathbf{K}^c]\{\mathbf{q}\} = \{\mathbf{f}\} \tag{20}$$

in which the superscript c denotes the convective matrix and

$$\overline{\mathbf{K}}_{IJ} = \int_{\Omega} \overline{\mathbf{C}}_I^{\mathrm{T}} \mathbf{k} \overline{\mathbf{C}}_J d\Omega \tag{21}$$

$$\mathbf{K}_{IJ}^{c} = \int_{\Gamma_3} h \mathbf{\Phi}_I^{\mathrm{T}} \mathbf{\Phi}_J d\Gamma \tag{22}$$

$$\mathbf{f}_I = \int_{\Omega} \mathbf{\Phi}_I^{\mathrm{T}} Q_v d\Omega - \int_{\Gamma_2} \mathbf{\Phi}_I^{\mathrm{T}} q_\Gamma d\Gamma + \int_{\Gamma_3} h T_a \mathbf{\Phi}_I^{\mathrm{T}} d\Gamma \tag{23}$$

$$\overline{\mathbf{C}}_I = \left\{ \bar{\mathbf{g}}_{Ix} \quad \bar{\mathbf{g}}_{Iy} \quad \bar{\mathbf{g}}_{Iz} \right\}^{\mathrm{T}} \tag{24}$$

where $\bar{\mathbf{g}}_{Ix}$, $\bar{\mathbf{g}}_{Iy}$, and $\bar{\mathbf{g}}_{Iz}$ are the x, y, and z components of the smoothed temperature gradient for node I, respectively.

After obtaining the nodal temperature from solving Eq. (20), the strain of thermal expansion induced by the variation in temperature becomes the initial strain $\boldsymbol{\varepsilon}_0$,

$$\boldsymbol{\varepsilon}_0 = \left\{ \alpha_x \Delta T \quad \alpha_y \Delta T \quad \alpha_z \Delta T \quad 0 \quad 0 \quad 0 \right\}^{\mathrm{T}} \tag{25}$$

where α_i $(i = x,\ y,\ x)$ is the thermal expansion coefficient in the ith direction. The relation between the thermal stress and strain can be expressed as

$$\bar{\boldsymbol{\sigma}} = \mathbf{D}(\bar{\boldsymbol{\varepsilon}} - \boldsymbol{\varepsilon}_0) \tag{26}$$

where $\bar{\boldsymbol{\varepsilon}}$ and $\bar{\boldsymbol{\sigma}}$ are vectors containing the smoothed strains and stresses, respectively, and $\mathbf{D}$ is the matrix of material constants that is in general anisotropic [35]. For isotropic materials, $\mathbf{D}$ contains only Young's modulus E and Poisson's ratio ν.

$$\mathbf{D} = \frac{E}{2(1+\nu)(1-2\nu)} \begin{bmatrix} 2(1-\nu) & 2\nu & 2\nu & 0 & 0 & 0 \\ 2\nu & 2(1-\nu) & 2\nu & 0 & 0 & 0 \\ 2\nu & 2\nu & 2(1-\nu) & 0 & 0 & 0 \\ 0 & 0 & 0 & 1-2\nu & 0 & 0 \\ 0 & 0 & 0 & 0 & 1-2\nu & 0 \\ 0 & 0 & 0 & 0 & 0 & 1-2\nu \end{bmatrix} \tag{27}$$

In the standard weak formulation, the potential (strain) energy of the thermoelastic system can be given by

$$\Pi(\mathbf{u}) = \frac{1}{2} \int_{\Omega} \boldsymbol{\varepsilon}^{\mathrm{T}} \mathbf{D} \boldsymbol{\varepsilon} d\Omega - \int_{\Omega} \boldsymbol{\varepsilon}^{\mathrm{T}} \mathbf{D} \boldsymbol{\varepsilon}_0 d\Omega - \int_{\Gamma t} \mathbf{u}^{\mathrm{T}} t_\Gamma d\Gamma \tag{28}$$

where the strains are the so-called compatible strains obtained using the (linear) kinematics relation of the strains and the displacements. The variational form can

be expressed as

$$\delta\Pi(\mathbf{u}) = \int_{\Omega} (\delta\boldsymbol{\varepsilon})^{\mathrm{T}} \mathbf{D}\boldsymbol{\varepsilon} d\Omega - \int_{\Omega} (\delta\boldsymbol{\varepsilon})^{\mathrm{T}} \mathbf{D}\boldsymbol{\varepsilon}_0 d\Omega - \int_{\Gamma_t} (\delta\mathbf{u})^{\mathrm{T}} t_{\Gamma} d\Gamma = 0 \tag{29}$$

In our formulation, the compatible strain $\boldsymbol{\varepsilon}$ in Eq. (29) is replaced by the smoothed strain $\bar{\boldsymbol{\varepsilon}}$ that satisfies the generalized (smoothed) Galerkin weak form that can be derived from the Hellinger-Reissner's two-field variational principle. The smoothed Galerkin weak form for our thermoelastic problems can be written as,

$$\delta\Pi(\mathbf{u}) = \int_{\Omega} (\delta\bar{\boldsymbol{\varepsilon}})^{\mathrm{T}} \mathbf{D}\bar{\boldsymbol{\varepsilon}} d\Omega - \int_{\Omega} (\delta\bar{\boldsymbol{\varepsilon}})^{\mathrm{T}} \mathbf{D}\boldsymbol{\varepsilon}_0 d\Omega - \int_{\Gamma_t} (\delta\mathbf{u})^{\mathrm{T}} t_{\Gamma} d\Gamma = 0 \tag{30}$$

Substituting Eq. (7) into Eq. (30), the discretized system equations for thermoelastic problems can be expressed in the following matrix form.

$$[\overline{\mathbf{K}}^{u}]\{\mathbf{d}\} = \{\overline{\mathbf{F}}\} \tag{31}$$

where

$$\overline{\mathbf{K}}^{u}_{IJ} = \int_{\Omega} \overline{\mathbf{B}}_I^{\mathrm{T}} \mathbf{D} \overline{\mathbf{B}}_J d\Omega \tag{32}$$

$$\overline{\mathbf{F}}_I = \int_{\Gamma_t} \boldsymbol{\Phi}_I^{\mathrm{T}} t_{\Gamma} d\Gamma + \int_{\Omega} \overline{\mathbf{B}}_I^{\mathrm{T}} \mathbf{D}\boldsymbol{\varepsilon}_0 d\Omega \tag{33}$$

in which $\overline{\mathbf{B}}$ is the smoothed strain matrix that is obtained through the gradient smoothing operation, and the superscript u denotes the stiffness matrix associated with the displacement field of a given discretization. To obtain the smoothed stiffness matrix of thermoelastic system, the nodal integration scheme with node-based gradient smoothing technique will be used to perform the domain integration, which will be detailed in the following section.

3.3. Gradient Smoothing Over Node-Based Smoothing Domains

To carry out the domain integration required in Eqs. (21) and (32), a set of node-based nonoverlapping sub-domains is created on top of the background mesh of 4-node tetrahedrons used for shape function construction. This set of sub-domains is also used for the gradient smoothing, and hence called smoothing domains. Based on the tetrahedral mesh, N smoothing domains $\Omega_k (k = 1, 2, \ldots, N)$ centered by node k can be formed. Figure 2 shows a typical nodal smoothing domain for one node and the details on the formation is illustrated in Figure 3. The smoothing domain of the interested node k is constructed by connecting sequentially the mid-edge-points, the centroids of the surface triangles, and the centroids of the sample cell I. The boundary of the smoothing domain Ω_k is labeled as Γ_k and the union of all Ω_k forms the global domain Ω exactly. Using this set of node-based smoothing domains, the domain integration in Eqs. (21) and (32)

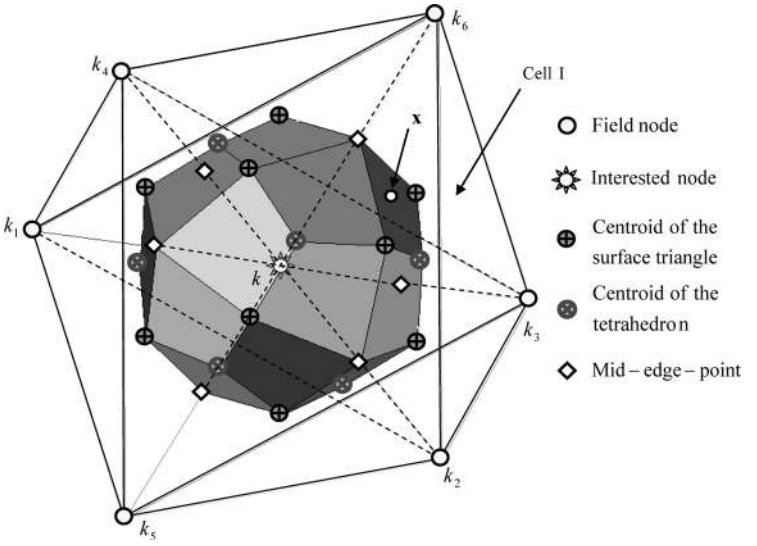

Figure 2. A typical 3-D node-based smoothing domain for node k formed by sequentially connecting the mid-edge-points, centroids of surface triangles, and centroids of eight surrounding four-node tetrahedrons.

becomes simple summation for all the smoothing domains, and the ''stiffness'' matrices can be further expressed as

$$\overline{\mathbf{K}}_{IJ} = \sum_{k=1}^{N} \overline{\mathbf{K}}_{IJ}^{(k)} \tag{34}$$

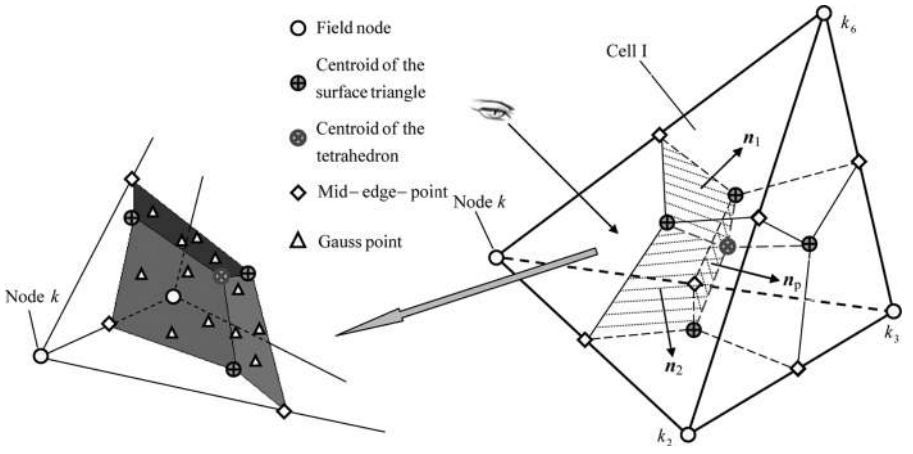

Figure 3. The schematic of one partition of the node-based smoothing domain for node k as one vertex of four-node tetrahedral cell I (k-k_2-k_3-k_6).

The sub-stiffness matrices for node k has the form of

$$\overline{\mathbf{K}}_{IJ}^{(k)} = \int_{\Omega_k} \overline{\mathbf{C}}_I^{\mathrm{T}} \, \mathbf{k} \, \overline{\mathbf{C}}_J \, d\Omega \tag{36}$$

$$\overline{\mathbf{K}}_{IJ}^{u(k)} = \int_{\Omega_k} \overline{\mathbf{B}}_I^{\mathrm{T}} \, \mathbf{D} \, \overline{\mathbf{B}}_J \, d\Omega \tag{37}$$

The gradient smoothing operation [17] is now performed over the smoothing domains, which yields the following smoothed gradient.

$$\bar{\varepsilon}_{IJ}^h(\mathrm{x}_k) = \int_{\Omega_k} \varepsilon_{IJ}^h(\mathrm{x}) \; W(\mathrm{x} - \mathrm{x}_k) \; d\Omega \tag{38}$$

where $\boldsymbol{\varepsilon}_{IJ}^h$ is the compatible gradient and W is a smoothing function given by

$$W(\mathrm{x} - \mathrm{x}_k) = \begin{cases} 1/V_k & \mathrm{x} \in \Omega_k \\ 0 & \mathrm{x} \notin \Omega_k \end{cases} \tag{39}$$

where $V_k = \int_{\Omega_k} d\Omega$ is the volume of smoothing domain for node k, as shown in Figure 2. Substituting Eq. (39) into Eq. (38) and integrating by parts, the smoothed gradient can become

$$\begin{aligned} \bar{\boldsymbol{\varepsilon}}_{IJ}^h(\mathrm{x}_k) &= \frac{1}{V_k} \int_{\Omega_\mathbf{k}} \varepsilon_{IJ}^h(\mathrm{x}) \; d\Omega \\ &= \frac{1}{V_k} \int_{\Omega_k} \frac{1}{2} \left(\frac{\partial u_I^h}{\partial x_J} + \frac{\partial u_J^h}{\partial x_I} \right) d\Omega \\ &= \frac{1}{2V_k} \int_{\Gamma_k} (u_I^h n_J + u_J^h n_I) d\Gamma \end{aligned} \tag{40}$$

where Γ_k is the boundary of the smoothing domain for node k.

Using the PIM shape functions for the temperature and displacement interpolations in the form of Eq. (7), the smoothed strain and temperature gradient for node k can be further expressed in the following matrix form, respectively, as

$$\bar{\boldsymbol{\varepsilon}}^h(\mathbf{x}_k) = \sum_{I \in D_k} \bar{\mathbf{B}}_I(\mathbf{x}_k) \mathbf{U}_I \tag{41}$$

$$\overline{\mathbf{g}}^h(\mathbf{x}_k) = \sum_{I \in D_k} \overline{\mathbf{C}}_I(\mathbf{x}_k) \mathbf{q}_I \tag{42}$$

where D_k is the number of total nodes associated with the smoothing domain of node k. For three-dimensional spaces, the corresponding expressions are

$$\overline{\mathbf{g}} = \{\bar{g}_x \; \bar{g}_y \; \bar{g}_z\}^{\mathrm{T}} \qquad \bar{\boldsymbol{\varepsilon}} = \{\bar{\varepsilon}_x \; \bar{\varepsilon}_y \; \bar{\varepsilon}_z \; \bar{\varepsilon}_{xy} \; \bar{\varepsilon}_{yz} \; \bar{\varepsilon}_{xz}\}^{\mathrm{T}} \tag{43}$$

$$\mathbf{q}_I = \{T_I \ T_I \ T_I\}^{\mathrm{T}} \quad \mathbf{U}_I = \{U_{Ix} \ U_{Iy} \ U_{Iz}\}^{\mathrm{T}} \tag{44}$$

$$\overline{\mathbf{C}}_I = \begin{Bmatrix} \bar{b}_{Ix} & \bar{b}_{Iy} & \bar{b}_{Iz} \end{Bmatrix}^{\mathrm{T}} \quad \overline{\mathbf{B}}_I^{\mathrm{T}}(\mathrm{X}_k) = \begin{bmatrix} \bar{b}_{Ix} & 0 & 0 & \bar{b}_{Iy} & 0 & \bar{b}_{Iz} \\ 0 & \bar{b}_{Iy} & 0 & \bar{b}_{Ix} & \bar{b}_{Iz} & 0 \\ 0 & 0 & \bar{b}_{Iz} & 0 & \bar{b}_{Iy} & \bar{b}_{Ix} \end{bmatrix} \tag{45}$$

and

$$\bar{b}_{Ii} = \frac{1}{V_k} \int_{\Gamma_k} \varphi_I(\mathbf{x}) n_i(\mathbf{x}) d\Gamma \quad (i = x, y, z) \tag{46}$$

where $\varphi_I(\mathbf{x})$ is the PIM shape function for node I. It can be found that the volume integrals are now transformed into surface integrals involving only the shape function due to the use of the gradient smoothing technique. Such a transform is exact, as long as the shape functions are continuous in the problem domain (in an H space). Otherwise, it is an approximation (in a G space) [16].

Using Gauss integration along boundary surface Γ_k of the smoothing domain Ω_k, Eq. (46) can be finally written in the following summation.

$$\bar{b}_{Ii} = \frac{1}{V_k} \sum_{q=1}^{N_s} \left[\sum_{r=1}^{N_g} w_r \varphi_I(\mathbf{x}_{qr}) n_i(\mathbf{x}_q) \right] \tag{47}$$

where N_s is the number of segment surface on Γ_k, N_g is the number of total Gauss points used for each segment surface, and w_r is the weight corresponding to the Gauss point.

Using the smoothed gradient and strain shown in Eq. (45), and further assuming that the gradient is constant over the entire smoothing domain, the stiffness matrices for our thermoelasticity problems can be obtained by simple summation.

$$\overline{\mathbf{K}}_{IJ} = \sum_{L=1}^{N} \mathbf{C}_I^{\mathrm{T}}(\mathbf{x}_L) \, \mathbf{k} \, \overline{\mathbf{C}}_J(\mathbf{x}_L) V_L \tag{48}$$

$$\overline{\mathbf{K}}_{IJ}^{u} = \sum_{L=1}^{3N} \bar{\mathbf{B}}_I^{\mathrm{T}}(\mathrm{x}_L) D \bar{\mathbf{B}}_J(\mathrm{x}_L) V_L \tag{49}$$

where V_L is the volume of smoothing domain for given node L.

It can be easily observed from Eqs. (48) and (49) that the resultant linear system matrices are symmetric and banded (due to the compact supports of PIM shape functions), which implies that the discretized system equations can be solved efficiently. Note, that there is no increase in degrees of freedom in the NS-PIM model, and hence, the dimensions of the matrices for NS-PIM are exactly the same as those in the FEM so long the same mesh is used.

4. NUMERICAL EXAMPLES

Two mechanical components subjected to thermal and mechanical loads are analyzed using the present NS-PIM and examined in detail in terms of the accuracy, convergence, and important bound property of numerical solutions. For comparison, an in-house FEM code is also used to simulate the problem using the same meshes as NS-PIM. As the analytical solutions are not available for these problems, reference results are obtained using ABAQUS® with a very fine mesh for comparison purposes. The equivalent energy norm heat transfer problem [4] is defined as

$$U_T = \int_\Omega \bar{\mathbf{g}}^{\mathrm{T}} \mathbf{k} \bar{\mathbf{g}} \, d\Omega \tag{50}$$

where, in our current case, $\bar{\mathbf{g}}$ is the smoothed temperature gradient in Eq. (43).

The temperature effect can be measured in the form of thermal strain energy [36]

$$\begin{aligned} \mathrm{U}_d &= \frac{1}{2} \int_\Omega (\bar{\boldsymbol{\varepsilon}} - \boldsymbol{\varepsilon}_0)^{\mathrm{T}} \mathrm{d}\Omega \\ &= \frac{1}{2} \int_\Omega (\bar{\boldsymbol{\varepsilon}}^{\mathrm{T}} \mathbf{D} \bar{\boldsymbol{\varepsilon}} - 2 \bar{\boldsymbol{\varepsilon}}^{\mathrm{T}} \mathbf{D} \boldsymbol{\varepsilon}_0 + \boldsymbol{\varepsilon}_0^{\mathrm{T}} \mathbf{D} \boldsymbol{\varepsilon}_0) d\Omega \end{aligned} \tag{51}$$

where the first term in Eq. (51) is the smoothed stiffness matrix derived earlier, which is a bilinear functional that represents the mechanical strain energy in the system due to the thermal effect. The last term is a constant with respect to the assumed mechanical displacements and hence has no effect on the stationary state of the system. The middle term is a linear functional, and is to be assembled to the system as a global force vector representing the temperature load.

In our analysis, the thermal analysis is performed first to obtain the distribution of the temperature in the solid, and then the thermoelastic analysis is conducted for the distributions of displacement, strain, and von Mises stress as the consequences of both the thermal effect and external mechanical loads.

4.1. 3-D Conduction Beam

The first example considered here is a 3-D conduction beam subjected to thermal loads, as shown in Figure 4. The temperature T_Γ is prescribed onto the left surface, a heat flux q_Γ enters into the solid continuously from the right surface, and heat convection occurs between the bottom surface and the ambient with a convection coefficient h.

The beam is also loaded with mixed mechanical pressure on the top surface, which varies in the form of $(-15 + 5000x^2)$Pa, as shown in Figure 5. The positive value in traction stands for the tensile and negative denotes the suctions. Note the essential boundary conditions of both temperature and displacement on the left surface can be imposed directly on the nodes thanks to the Delta function property of the PIM shape functions. The parameters used in the computation are: $L = 0.09$ m, $H = 0.009$ m, $B = 0.009$ m, $Q_{\mathrm{v}} = 0$, $k_1 = 15\,\mathrm{W/(m \cdot {}^\circ C)}$, $k_2 = 10\,\mathrm{W/(m \cdot {}^\circ C)}$,

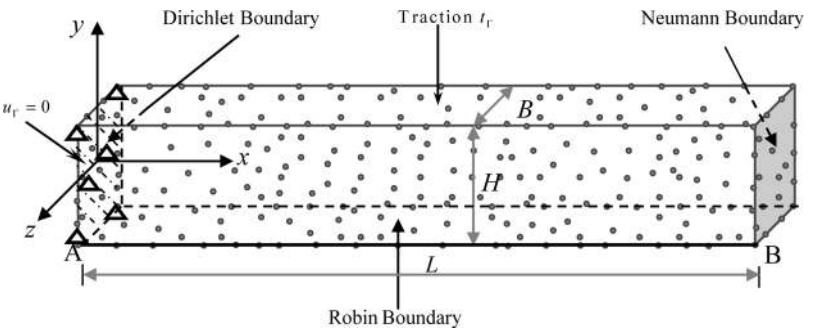

Figure 4. Discretized model of a 3-D beam subjected to thermal and mechanical loads.

$k_3 = 5\,\mathrm{W/(m \cdot {}^\circ C)}$, $h = 1500\,\mathrm{W/(m^2 \cdot {}^\circ C)}$, $T_\Gamma = 0$, $T_a = 400^\circ\mathrm{C}$, $q_\Gamma = -2000\,\mathrm{W/m^2}$, $u_\Gamma = 0$, $\alpha_x = \alpha_y = \alpha_z = 1.02 \times 10^{-5}/^\circ\mathrm{C}$, $E = 3.0 \times 10^{10}$ Pa, and $\nu = 0.3$.

The problem domain is discretized with 1,042 irregularly distributed nodes to form the 4-node tetrahedrons (T4). The same mesh is used for both the NS-PIM model and our in-house FEM model. The reference solution is obtained using a very fine mesh with about 10 times more nodes.

4.1.1. Temperature Distribution. A heat transfer analysis is performed first, and the computed temperature values obtained using the present NS-PIM at the nodes on the bottom edge (marked as AB in Figure 4) are listed in Table 1, along with the results of linear FEM and the reference solution. It can be found that NS-PIM solutions are in very good agreement with the reference solutions, and have a similar accuracy as the FEM solutions. This shows that the NS-PIM model works well for this 3-D heat transfer problem. This finding is consistent with those made in previous studies [15, 20]; NS-PIM gives at least a similar accuracy for the results of primary variables (that is temperature in this case).

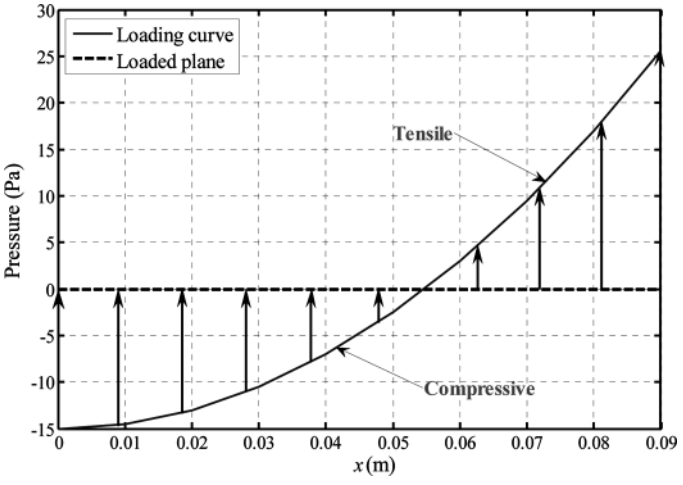

Figure 5. Mechanical loading curve: pressure on the top surface of the 3-D beam.

Table 1. Comparison of the solutions of nodal temperature (°C) along the AB edge for the 3-D beam problem

x (m)	0.003	0.012	0.021	0.030	0.039	0.048	0.057	0.660	0.075	0.084	0.090
Reference	228.84	357.56	388.73	396.99	399.23	399.81	399.96	400.03	400.19	400.73	401.92
NS-PIM	243.53	357.75	388.64	396.97	399.24	399.82	399.96	400.03	400.18	400.70	401.90
FEM	212.71	357.60	388.49	397.04	399.21	399.80	399.96	400.03	400.17	400.69	401.88

4.1.2. Thermal Deformation. After the temperature field is obtained, the initial strain resulted from the (free) thermal expansion can be obtained based on Eq. (25), and the temperature load is then added to the global load vector of the thermoelastic system. The NS-PIM is then used again to compute the deformation of the 3-D beam as a consequence of both the thermal and mechanical loads. Figures 6*a* and 6*b* show, respectively, the distribution of displacements in x and y directions, together with the reference solutions that are obtained using fine mesh with a total of 11,052 nodes.

It can be observed that the computed displacements match well with the reference, and the accuracy of linear NS-PIM is better than that from the linear FEM using the same 4-node tetrahedral mesh. This shows the effectiveness of the NS-PIM formulation for this 3-D thermoelastic problem.

Figure 7 shows the contours of displacement in the z-direction obtained from both NS-PIM and FEM, together with the reference obtained using irregularly distributed 14,873 nodes. It can be observed that the present results are in better agreement with the reference solution compared to those of the FEM when the same mesh is used. Note also that the largest displacement is in even better agreement with the reference solution compared to the FEM's solution.

4.1.3. Von Mises Stress. The von Mises criterion is the most commonly used for the assessment of stress failure of metal materials [33, 36]. The failure criterion states that the material will fail when the von Mises stress σ_{VM} exceeds the allowable

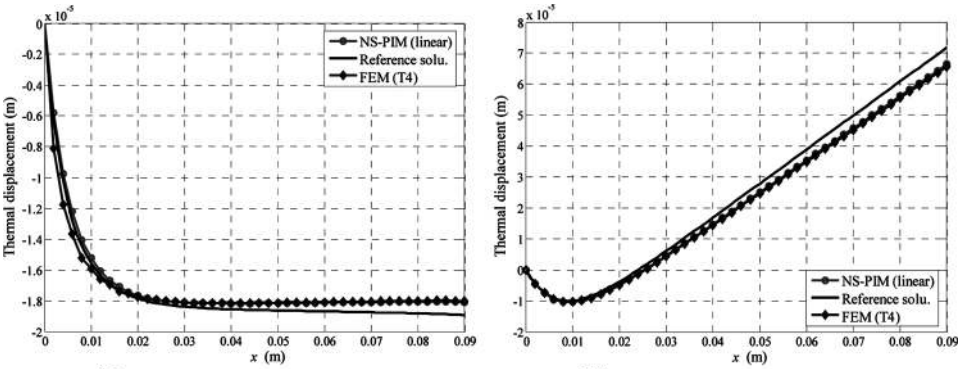

(*a*) Displacement in the x-direction. (*b*) Displacement in the y-direction.

Figure 6. Distribution of the displacement along edge AB on the 3-D beam subjected to thermal and mechanical loads.

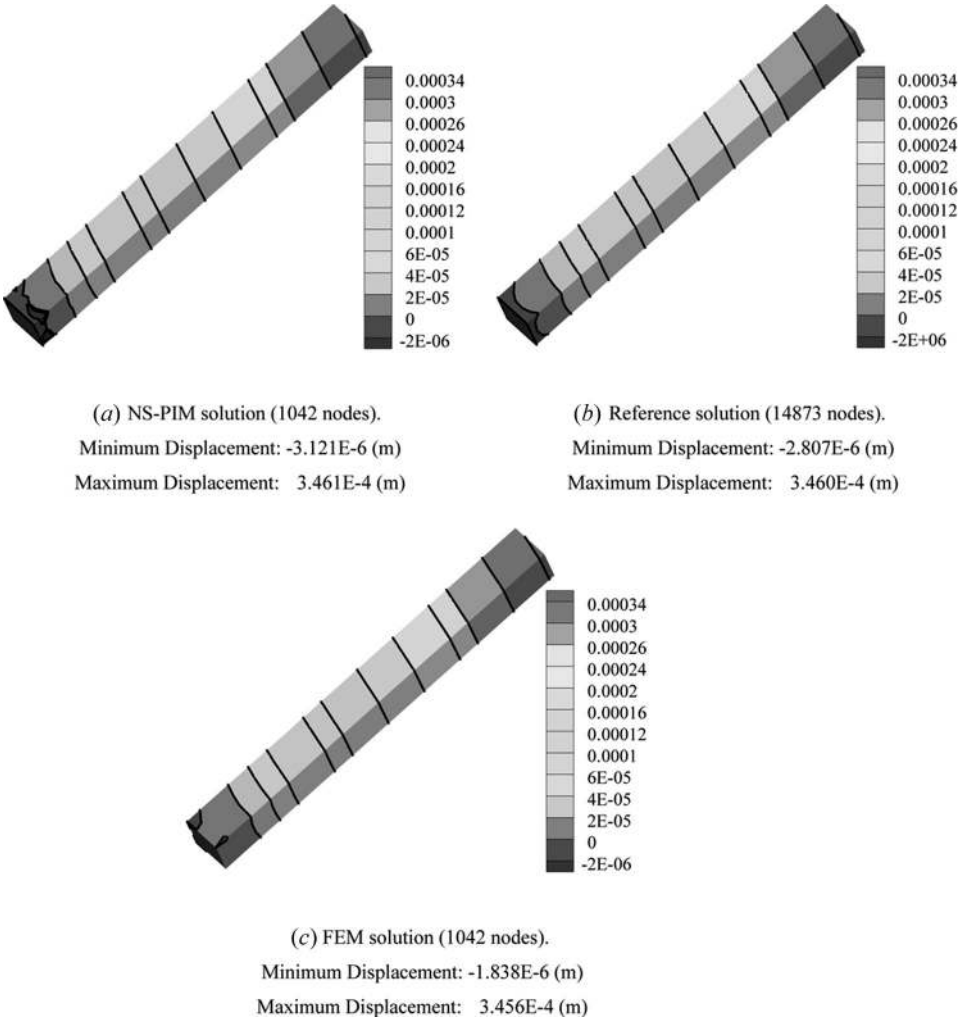

Figure 7. Comparisons of computed displacement field in the z-direction.

yield stress σ_Y of the given material. Hence we need to make sure at any point in the solid/structure that

$$\sigma_{VM} \leq \sigma_Y \tag{52}$$

The von Mises stress σ_{VM} is computed using

$$\sigma_{VM} \leq \sqrt{I_1^2 - 3I_2} \tag{53}$$

where $I_1$and I_2 are the first two invariants of the stress tensor. Using the values of stress components obtained numerically, $I_1$and I_2can be computed using

$$I_1 = \bar{\sigma}_x + \bar{\sigma}_y + \bar{\sigma}_z \tag{54}$$

$$I_2 = \bar{\sigma}_x\bar{\sigma}_y + \bar{\sigma}_y\bar{\sigma}_z + \bar{\sigma}_x\bar{\sigma}_z - \bar{\tau}_{xy}^2 - \bar{\tau}_{yz}^2 - \bar{\tau}_{xz}^2 \tag{55}$$

Figure 8 plots the contour of von Mises stress obtained using the NS-PIM, the reference means, and FEM. Figure 8 reveals that the present NS-PIM can obtain more accurate von Mises stress than FEM does, and the NS-PIM solution obtained using a very coarse mesh of 505 nodes agrees very well with the reference one.

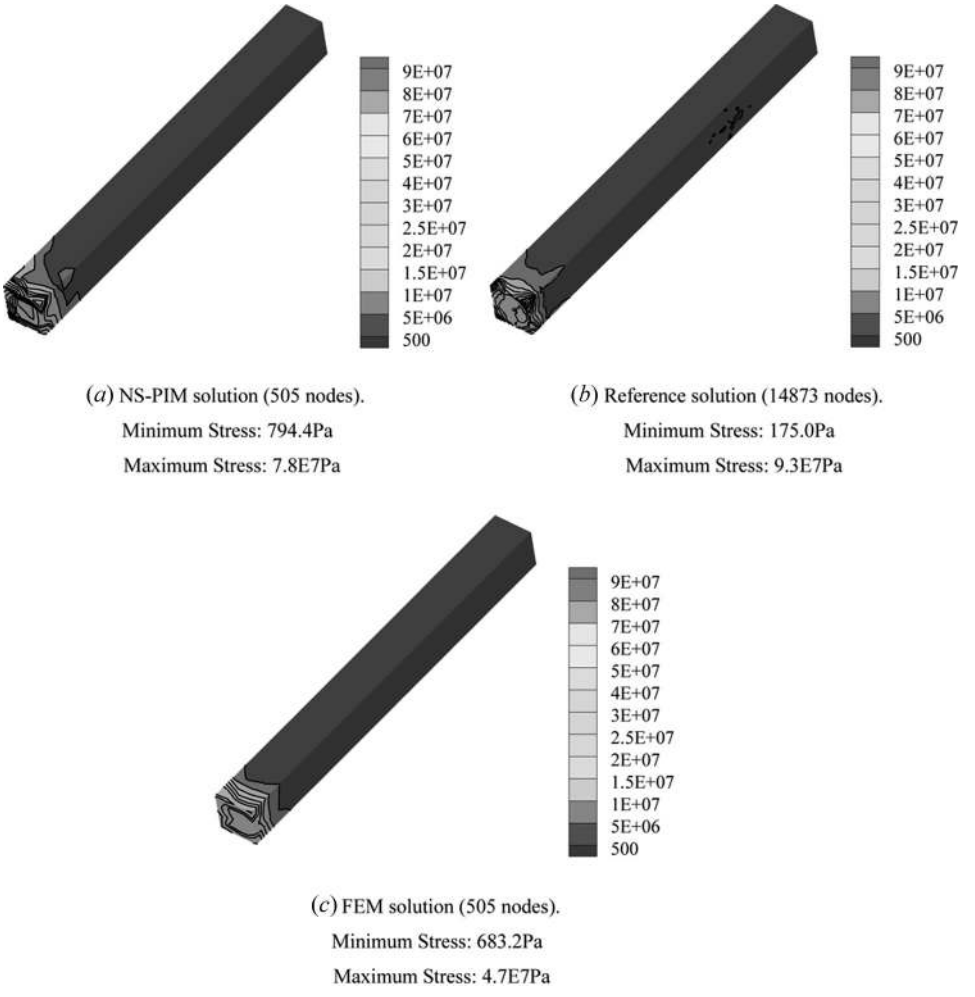

Figure 8. Comparisons of contours for nodal von Mises stress (σ_{VM}) in the 3-D beam.

Note that the present NS-PIM formulation is derived from the smoothed Galerkin weak form, in which the smoothed gradients ($\bar{\boldsymbol{\varepsilon}}$ and $\bar{\mathbf{g}}$) are obtained through Eqs. (41) and (42), respectively. The NS-PIM model so-constructed behaves softer compared with the FEM model [11], and hence can produce a more accurate and more smoothing solution for the gradients (strains and stresses). The similar phenomenon has also been observed in the analysis of solid mechanics [11, 15]. NS-PIM can obtain higher accuracy in stresses than the corresponding FEM model based on the same mesh.

4.1.4. Solution bound. It is well-known that the displacement-based fully compatible FEM always provides a lower bound [4] in the energy form of the exact solution to elastic problems with homogeneous essential boundary conditions. It is, however, much more difficult to bound the solution from above for thermoelasic problems, and the NS-PIM offers one effective means for the upper bound solution. To present the important bound property of NS-PIM, four models for the 3-D beam are created with irregularly distributed nodes of 505, 1,042, 1,667, and 2,858.

Figure 9 shows the convergence property of the equivalent energy for the temperature field with the increase of degree of freedoms (DOF) for both NS-PIM and FEM. The reference value is calculated using ABAQUS® with a very fine mesh of 14,873 nodes. It can be seen that the equivalent energy obtained using the NS-PIM model is larger than that of the reference solution; in comparison, the energy of the FEM model is smaller than the reference value. This finding confirms that the 3-D NS-PIM formulation provides an upper bound solution for the heat transfer problem [20], which is an important complement to the fully compatible FEM.

Figure 10 shows the convergence property in strain energy for the thermoelastic system; NS-PIM gives an upper bound and FEM gives a lower bound. The

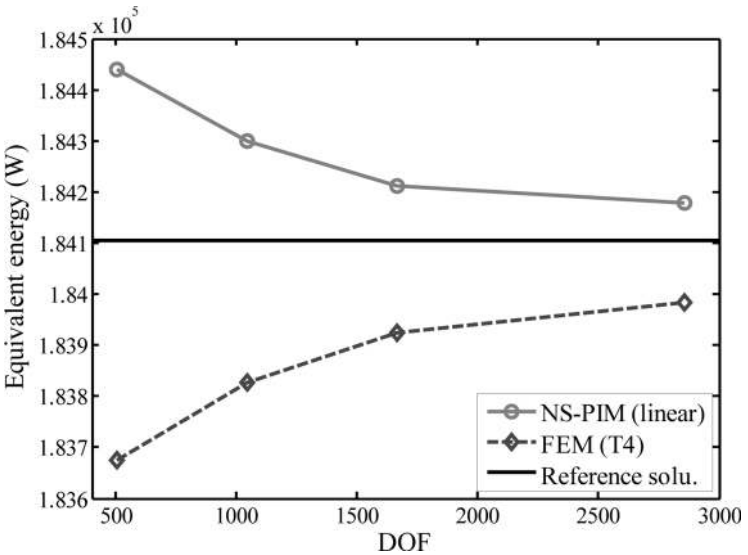

Figure 9. Upper and lower bound solutions in equivalent energy for the temperature field in the 3-D beam obtained using the present NS-PIM and FEM.

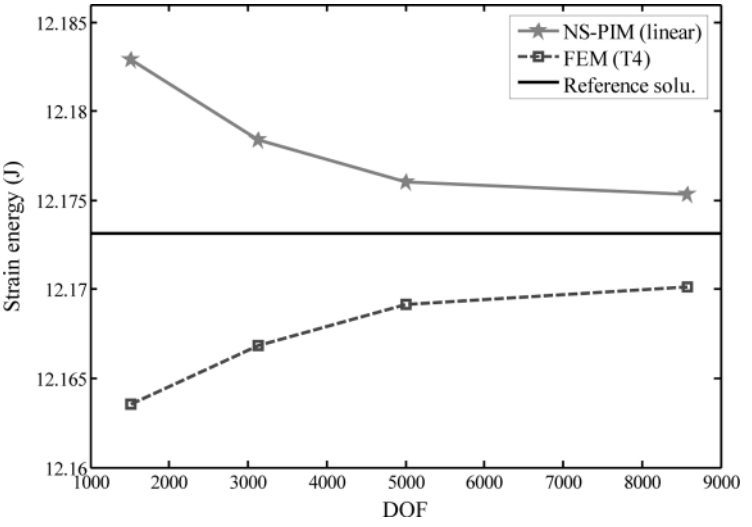

Figure 10. Upper and lower bound solutions in strain energy for 3-D thermoelastic beam obtained using the present NS-PIM and FEM.

thermal strain energy of the NS-PIM model is larger than the reference solution and converges from above with the increase in DOF (or mesh density). On the contrary, the corresponding FEM model approaches the exact model from below and obtains the lower bound solution for thermoelasticity problems with homogeneous essential boundary conditions in both temperature and displacement.

4.2. An Engine Pedestal

The following example comes from an actual aero-engine pedestal with a very complicated geometry, which is manufactured using the plasma

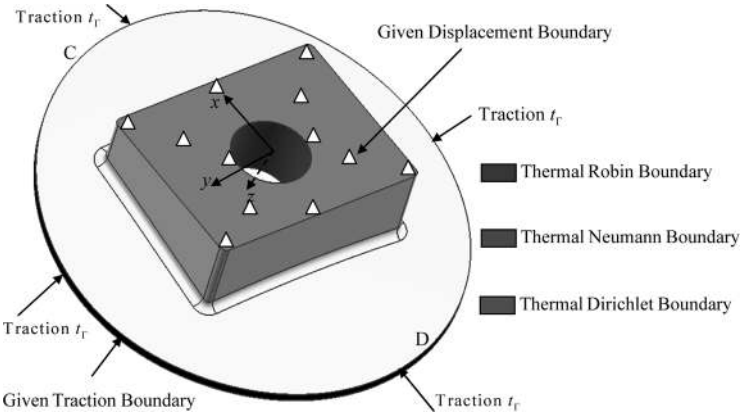

Figure 11. An engine pedestal subjected to Dirichlet, Neumann, and Robin conditions, respectively, on the baseplane, inner surface of installing hole, and circumferential surface of the cap structure. Displacement and traction boundary conditions are also applied on the baseplane and circumferential surface.

Table 2. Cartesian coordinates **x** (x, y, z) of the nine nodes located on the circumferential arc CD

ID.	1	2	3	4	5	6	7	8	9
x(m)	8.0E-3	6.8E-2	4.8E-2	2.5E-2	9.5E-3	1.4E-2	3.4E-2	5.7E-2	7.3E-2
y(m)	2.E-17	1.8E-2	3.2E-2	2.8E-2	9.8E-3	−1.8E-2	−3.2E-2	−2.8E-2	−4.9E-2
z(m)	4.1E-3	1.3E-2	8.8E-3	5.6E-3	4.2E-3	4.7E-3	6.5E-3	1.1E-2	1.4E-2

deposition-layered technique [31]. The pedestal part is made of superalloy material and the dimensions can be found in ref. [37]. A simplified model of pedestal part is shown in Figure 11.

The thermal loadings are also quite complicated and are given in the form of specified temperature, heat flux, and convection on different situations of the pedestal: the baseplane, inner surface of the installing hole, and the circumferential surface, as indicated by color codes in Figure 11. In addition, the pedestal is also subjected to mechanical loads in which the baseplane is fixed rigidly with zero displacement in three directions, and a constant traction of -5×10^5Pa is given to the circumferential surface to simulate the compressive effect of mechanical loads originated from other components and whole mechanical structures.

For quantitative comparison, the circumferential surface CD of the baseplane (marked in Figure 11) is divided evenly into eight segments, with nine observation points. The coordinates of the nine observation points on the circumferential arc edge CD are listed in Table 2. Computed values at these observation points will be output and examined in great detail. Other parameters used in the computation of the pedestal part are the same as those for the 3-D beam problem listed in Section 4.1.

4.2.1. Temperature distribution. The problem domain is discretized with a tetrahedral mesh of 587 nodes. The computed temperature values at these nine observation nodes are listed in Table 3, together with the FEM solution and the reference solution obtained using 12,344 nodes. It is found that the NS-PIM results of temperature are larger than the reference solutions, while the FEM solutions are smaller than the reference solutions. This attributes to the softening effect of the NS-PIM model induced by the gradient smoothing technique. These findings show again that together with FEM, the NS-PIM can bound the solution from both sides using the same elemental mesh.

4.2.2. Displacement field. Due to the combined action of thermal and mechanical loads, the displacement field within the pedestal is expected to be more complicated. Figure 12 shows the distribution of the displacements in the x and y directions along the circumferential arc CD. It is clearly seen that the solutions obtained from

Table 3. Comparisons of numerical solutions of temperature (°C) along the circumferential arc CD

ID.	1	2	3	4	5	6	7	8	9
Reference	318.39	296.45	321.51	323.97	317.94	318.47	327.04	310.64	296.75
NS-PIM	320.09	300.92	323.67	325.67	319.52	320.00	330.13	313.47	300.65
FEM	316.41	290.58	317.99	319.90	315.54	314.42	324.39	304.50	293.42

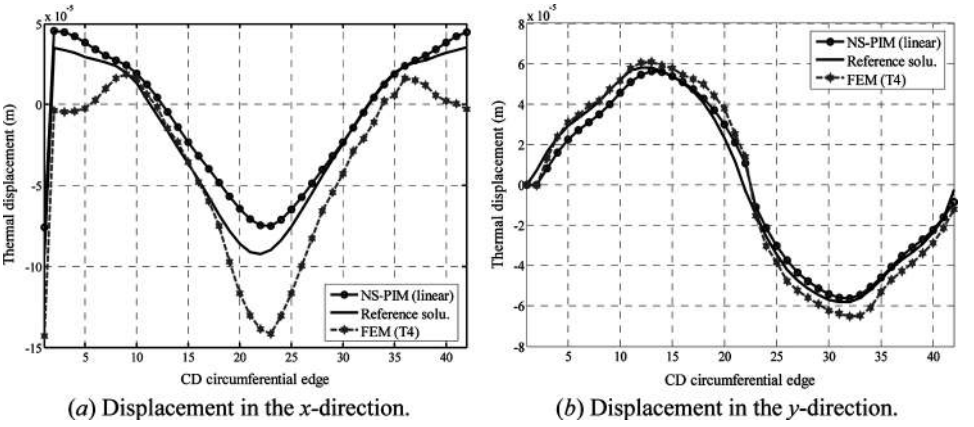

(*a*) Displacement in the *x*-direction. (*b*) Displacement in the *y*-direction.

Figure 12. Distribution of displacement along the circumferential arc CD on the pedestal subjected to both thermal and mechanical loads.

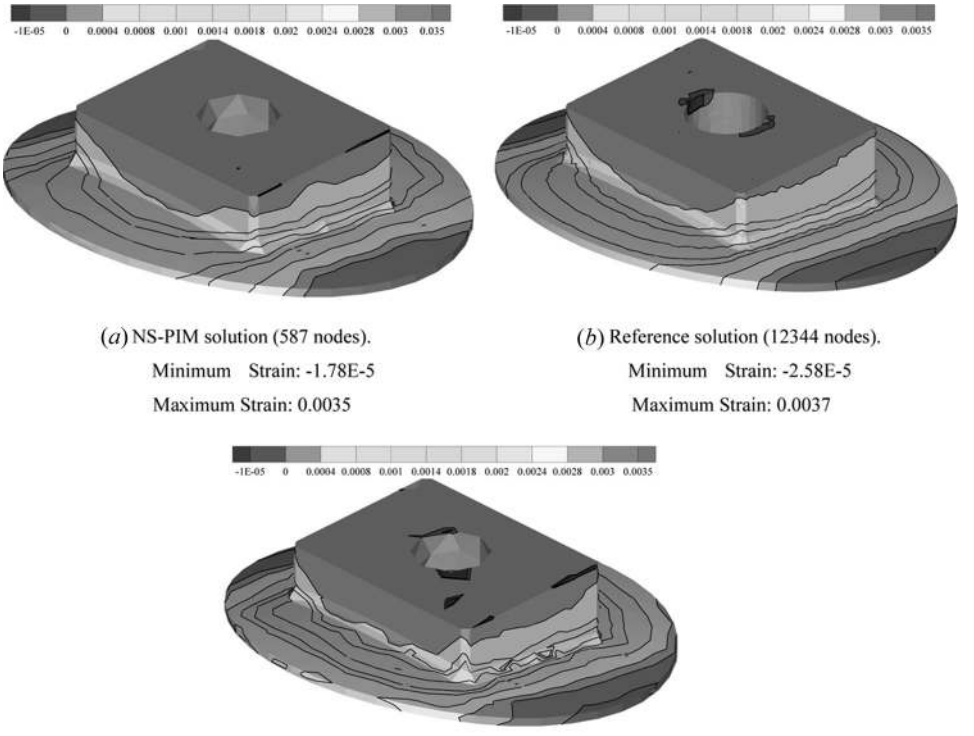

(*a*) NS-PIM solution (587 nodes).
Minimum Strain: -1.78E-5
Maximum Strain: 0.0035

(*b*) Reference solution (12344 nodes).
Minimum Strain: -2.58E-5
Maximum Strain: 0.0037

(*c*) FEM solution (587 nodes).
Minimum Strain: -6.48E-5
Maximum Strain: 0.0038

Figure 13. Comparisons of computed thermal strain.

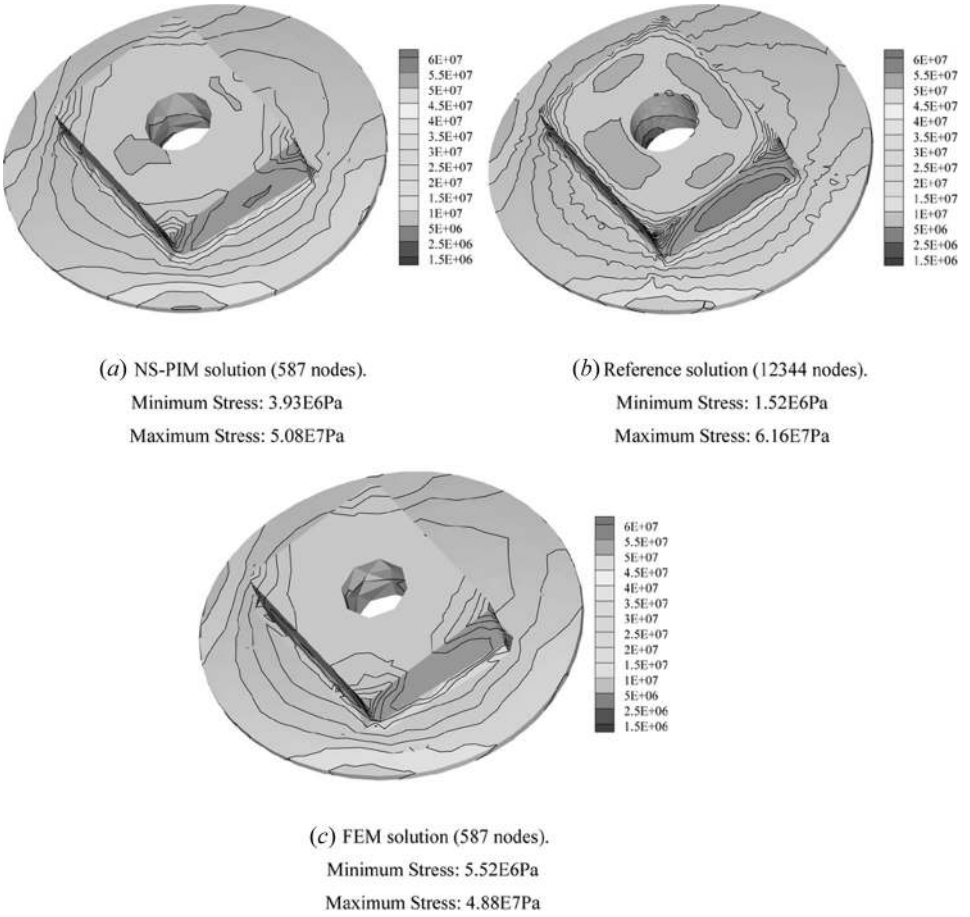

Figure 14. Comparisons of computed von Mises stress.

the NS-PIM agree well with the reference solutions (obtained using 11,636 nodes), and much better than FEM using the same 4-node tetrahedral mesh.

4.2.3. Strain and von Mises stress. Figure 13 shows the contours of strain fields obtained using NS-PIM, FEM of the same mesh, and the reference solution. It is observed that the contour lines of NS-PIM solutions are smoother than those of FEM. The NS-PIM results are also much closer to the reference results, compared with that of the FEM.

Figure 14 demonstrates the comparison of the resultant von Mises stress contour in the pedestal. It can be clearly seen that the NS-PIM solution, especially for the nodal peak von Mises stress within high-gradient region, agrees better with the reference one compared with the FEM solution using the same coarse mesh.

4.2.4. Solution bound. Figures 9 and 10 show that the NS-PIM solution (in both equivalent energy for heat transfer and strain energy for thermoelasticity) is larger than the reference solution. The reference solution is, on the other hand,

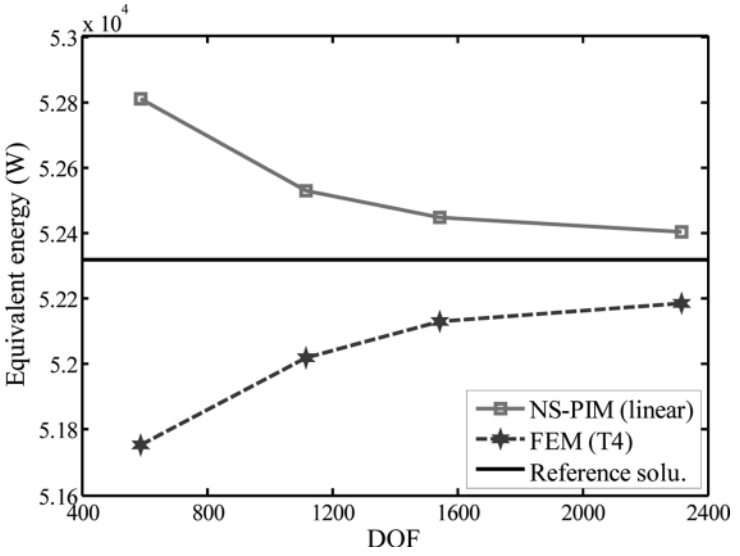

Figure 15. Upper and lower bound solutions in equivalent energy for the temperature field in the 3-D pedestal.

larger than that of the displacement-based fully compatible FEM. This bound property of NS-PIM model is of practical importance in providing certified solutions for engineering problems, and hence is examined in detail in the 3-D beam problem. To further confirm the upper bound property of the present NS-PIM for more complicated thermoelastic systems, four discretized models of the pedestal

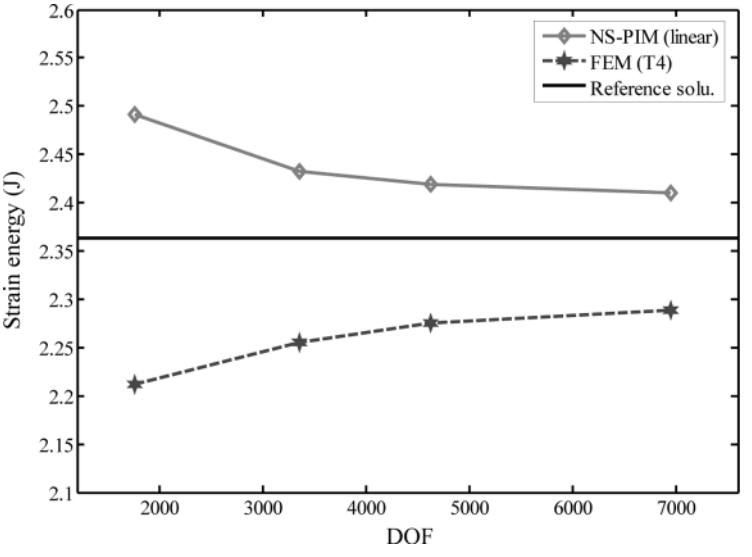

Figure 16. Upper and lower bound solutions in strain energy for 3-D pedestal.

are created with irregularly distributed 587, 1,117, 1,543, and 2,315 nodes. Figure 15 plots the numerical solutions (in equivalent energy norm for the temperature field) against the DOFs for both NS-PIM and FEM. The reference solution is obtained using the FEM with a very fine mesh of 12,344 nodes. It can be observed again that the present NS-PIM produces an upper bound solution in equivalent energy for this very complicated problem with homogenous essential boundary conditions ($T_\Gamma = 0$). The solution converges to the reference solution from above with the increase of DOFs.

Figure 16 plots the convergence state of numerical solutions in thermal strain energy for this complicated pedestal problem with homogenous essential boundary conditions ($u_\Gamma = 0$). It can be seen that the present NS-PIM also provides an upper bound solution in thermal strain energy. The upper bound property of the NS-PIM implies that even for the primary variables (nodal temperature **q** in Eq. (20) and nodal displacement **d** in Eq. (31)) the solution can also be larger than that of the exact model under certain conditions. This has been observed in both Tables 1 and 3, where the values are all positive (and hence has the same feature of an energy norm).

Figures 9, 10, 15, and 16 indicate that with the increase of DOF, both equivalent energy for the temperature field and the strain energy for thermoelasticity obtained from NS-PIM and FEM all converge to the referencesolution from above and below, respectively. This important property allows engineers to verify a numerical solution and conduct the adaptive analysis for solutions of the desired accuracy for complicated solids and structures subjected to complicated thermal and mechanical loads when the analytical solutions are difficult to obtain. Moving forward, one can even attempt to obtain exact solutions in certain norms using only finite mesh, by properly combining softer and stiffer models, as reported in refs. [38, 39].

5. CONCLUSIONS

In this work, the NS-PIM is further formulated for 3-D thermoelastic problems with complex geometric shape and complicated boundary conditions under the varied thermal and mechanical loads. In this approach, polynomial basis functions are utilized to construct the PIM shape functions using the point interpolation procedure. The smoothed Galerkin weak form is then adopted to create the discretized system equations. Examples of 3-D complex thermoelastic problems are analyzed to examine the accuracy, convergence, and the very important upper bound property of NS-PIM. Several concluding remarks can be made from our detailed study.

1. No derivatives of shape functions are required due to the use of the gradient smoothing technique, which can result in more accurate gradient solutions even using low-order shape functions.
2. Shape functions generated using the point interpolation method possess the Kronecker Delta function property, and hence allow the straightforward treatment of essential boundary conditions.
3. The present NS-PIM can achieve higher accuracy in von Mises stress compared with FEM, using the same lower-order shape functions.

4. For the first time, the upper bound solutions in both equivalent energy norm for heat transfer and thermal strain energy norm for thermoelasticity are obtained using the NS-PIM for 3-D thermoelastic problems with homogeneous essential boundary conditions. Together with the standard FEM, we now have a simple means to bound the solution for thermoelastic problems from both below and above using the same tetrahedral mesh.

In order to analyze the time-dependent problems, an efficient edge-based smoothed point interpolation method (ES-PIM) [40] has been proposed recently for solid mechanics. The meshfree ES-PIM is then further formulated for transient linear and nonlinear heat transfer problems.

REFERENCES

1. G. R. Liu, *Meshfree Methods: Moving Beyond the Finite Element Method*, CRC Press, Boca Raton, Florida, 2002.
2. J. N. Reddy and D. K. Gartling, *The Finite Element Method in Heat Transfer and Fluid Dynamics*, 2nd ed., CRC Press, Boca Raton, Florida, 2001.
3. G. R. Liu and S. S. Quek, *Finite Element Method: A Practical Course*, Butter-worth-heinemann, Burlington, Massachassetts, 2003.
4. O. C. Zienkiewicz and R. L. Taylor, *The Finite Element Method*, 5th ed., Butterworth-Heinemann, Oxford, 2000.
5. G. R. Liu and G. Y. Zhang, Upper Bound Solution to Elasticity Problems: A Unique Property of the Linearly Conforming Point Interpolation Method (LC-PIM), *Int. J. Numer. Meth. Eng.*, vol. 74, no. 7, pp. 1128–1161, 2008.
6. L. B. Lucy, A Numerical Approach to Testing of the Fission Hypothesis, *Astron. J.*, vol. 8, no. 12, pp. 1013–1024, 1977.
7. J. J. Monaghan, An Introduction to SPH, *Comput. Phys. Commun.*, vol. 48, no. 1, pp. 89–96, 1998.
8. T. Belytschko, Y. Y. Lu, and L. Gu, Element-Free Galerkin Method, *Int. J. Numer. Meth. Eng.*, vol. 37, no. 2, pp. 229–256, 1994.
9. W. K. Liu, S. Jun, and Y. F. Zhang, Reproducing Kernel Particle Methods, *Int. J. Numer. Meth. Fluids*, vol. 20, no. 8–9, pp. 1081–1106, 1995.
10. S. N. Atluri and T. Zhu, A New Meshless Local Petrov-Galerkin (MLPG) Approach in Computational Mechanics, *Comput. Mech.*, vol. 22, no. 2, pp. 117–127, 1998.
11. G. R. Liu, G. Y. Zhang, K. Y. Dai, Y. Y. Wang, Z. H. Zhong, G. Y. Li, and X. Han, A Linearly Conforming Point Interpolation Method (LC-PIM) for 2-D Solid Mechanics Problems, *Int. J. Comput. Meth.*, vol. 2, no. 4, pp. 645–665, 2005.
12. G. R. Liu and Y. T. Gu, *An Introduction to Meshfree Methods and Their Programming*, Springer, Dordrecht, The Netherlands, 2005.
13. J. G. Wang and G. R. Liu, A Point Interpolation Meshless Method Based on the Radial Basis Functions, *Int. J. Numer. Meth. Eng.*, vol. 54, no. 11, pp. 1623–1648, 2002.
14. G. R. Liu, Y. Li, K. Y. Dai, M. T. Luan, and W. Xue, A Linearly Conforming Radial Point Interpolation Method for Solid Mechanics Problems, *Int. J. Comput. Meth.*, vol. 3, no. 4, pp. 401–428, 2006.
15. G. Y. Zhang, G. R. Liu, Y. Y. Wang, H. T. Huang, Z. H. Zhong, G. Y. Li, and X. Han, A Linearly Conforming Point Interpolation Method (LC-PIM) for Three-Dimensional Elasticity Problems, *Int. J. Numer. Meth. Eng.*, vol. 72, no. 13, pp. 1524–1543, 2007.

16. G. R. Liu, A Generalized Gradient Smoothing Technique and the Smoothed Bilinear Form for Galerkin Formulation of a Wide Class of Computational Methods, *Int. J. Comput. Meth.*, vol. 5, no. 2, pp. 199–236, 2008.
17. J. S. Chen, C. T. Wu, S. Yoon, and Y. A. You, A Stabilized Conforming Nodal Integration for Galerkin Meshfree Methods, *Int. J. Numer. Meth. Eng.*, vol. 50, no. 2, pp. 435–466, 2001.
18. S. Beissel and T. Belytschko, Nodal Integration of the Element-Free Galerkin Method, *Comput. Methods Appl. Meth. Engrg.*, vol. 139, no. 1, pp. 49–74, 1996.
19. S. C. Wu, G. R. Liu, H. O. Zhang, X. Xu, and Z. R. Li, A Node-Based Smoothed Point Interpolation Method (NS-PIM) for Three-Dimensional Heat Transfer Problems, *Int. J. Therm. SCI.*, in press, 2008.
20. S. C. Wu, G. R. Liu, H. O. Zhang, and G. Y. Zhang, A Node-Based Smoothed Point Interpolation Method (NS-PIM) for Thermoelastic Problems with Solution Bounds, *Int. J. Heat Mass Tran.*, in press, 2008.
21. G. Y. Zhang, G. R. Liu, T. T. Nguyen, C. X. Song, X. Han, Z. H. Zhong, and G. Y. Li, The Upper Bound Property for Solid Mechanics of the Linearly Conforming Radial Point Interpolation Method (LC-RPIM), *Int. J. Comput. Meth.*, vol. 4, no. 3, pp. 521–541, 2007.
22. G. R. Liu and Z. H. Tu, An Adaptive Procedure Based on Background Cells for Meshfree Methods, *Comput. Methods Appl. Meth. Engrg.*, vol. 191, no. 17–18, pp. 1923–1943, 2002.
23. G. Y. Zhang and G. R. Liu, An Efficient Adaptive Analysis Procedure for Certified Solutions with Exact Bounds of Strain Energy for Elastic Problems, *Finite Elem. Anal. Des.*, vol. 44, no. 14, pp. 831–841, 2008.
24. G. R. Liu, X. Xu, G. Y. Zhang, and Y. T. Gu, An Extended Galerkin Weak Form and a Point Interpolation Method with Continuous Strain Field and Superconvergence Using Triangular Mesh, *Comput. Mech.*, in press, 2008.
25. G. R. Liu, T. Nguyen-Thoi, H. Nguyen-Xuan, and K. Y. Lam, A Node-Based Smoothed Finite Element Method (NS-FEM) for Upper Bound Solutions to Solid Mechanics Problems, *Comput. Struct.*, in press, 2008.
26. G. R. Liu, A Weakened Weak (W^2) Form for a Unified Formulation of Compatible and Incompatible Displacement Methods, *Int. J. Numer. Meth. Eng.*, in press, 2008.
27. G. R. Liu, T. Nguyen-Thoi, and K. Y. Lam, An Edge-Based Smoothed Finite Element Method (ES-FEM) for Static Free and Vibration Analyses in Solids, *J. Sound. Vib.*, in press, 2008.
28. X. Y. Cui, G. R. Liu, G. Y. Li, X. Zhao, T. Nguyen-Thoi, and G. Y. Sun, A Smoothed Finite Element Method (SFEM) for Linear and Geometrically Nonlinear Analysis of Plates and Shells, *CMES: Comp. Model. Eng.*, vol. 28, no. 2, pp. 109–125, 2008.
29. Y. Jaluria and K. E. Torrance, *Computational Heat Transfer*, 2nd ed., Taylor & Francis, London, 2003.
30. S. C. Wu, H. O. Zhang, Q. Tang, L. Chen, and G. L. Wang, Meshless Analysis of the Substrate Temperature in Plasma Spraying Process, *Int. J. Therm. SCI.*, in press, 2008.
31. S. C. Wu, G. L. Wang, H. O. Zhang, and X. H. Xiong, Plasma Deposition Dieless Manufacturing of Turbine Parts: Thermal Stress Control and Process Optimization, *Trans. China Welding Institution*, vol. 28, no. 6, pp. 49–52, 56, 2007.
32. P. Lancaster and K. Salkauskas, Surfaces Generated by Moving Least Square Methods, *Math. Comput.*, vol. 37, no. 155, pp. 141–158, 1981.
33. I. M. Smith and D. V. Griffiths, *Programming the Finite Element Method*, 2nd ed., John Wiley, New York, 1988.
34. T. R. J. Hughes, *The Finite Element Method*, Prentice-Hall, London, 1987.
35. G. R. Liu and Z. C. Xi, *Elastic Waves in Anisotropic Laminates*, CRC Press, Boca Raton, FL, 2001.

36. T. R. Chandrupatla and A. D. Belegundu, *Introduction to Finite Elements in Engineering*, 3rd ed., Prentice Hall, New Jersey, 2002.
37. G. L. Wang, S. C. Wu, and H. O. Zhang, Numerical Simulation of Temperature Field on Complicated Parts During Plasma Deposition Dieless Manufacturing, *Trans. China Welding Institution*, vol. 28, no. 5, pp. 49–52, 2007.
38. G. R. Liu, T. Nguyen-Thoi, and K. Y. Lam, A Novel FEM by Scaling the Gradient of Strains with Factor (αFEM), *Comput. Mech.*, 2008, in press.
39. G. R. Liu, T. Nguyen-Thoi, and K. Y. Lam, A Novel Alpha Finite Element Method (αFEM) for Exact Solution to Mechanics Problems Using Triangular and Tetrahedral Elements, *Comput. Methods Appl. Meth. Engrg.*, vol. 197, nos. 45–48, pp. 3883–3897.
40. G. R. Liu and G. Y. Zhang, Edge-based Smoothed Point Interpolation Methods, *Int. J. Comput. Meth.*, in press, 2008.